Optimization of the Multi-Level Spring Restrainer for Bridges by Hybrid Particle Swarm and Gravitational Search Algorithm

Mustafa Kareem Hamzah[1,2] · **Farzad Hejazi**[3] · **Najad Ayyash**[1]

Abstract

This paper proposes a new multi-level spring restrainer (MLSR) that exhibits multi stiffness performance in different levels of movement of bridge superstructure to prevent unseating during applied dynamic loads. The analytical model of the proposed MLSR was formulated and the fabricated prototype was tested using dynamic actuator. Based on the developed analytical mode, the function of MLSR device relied on 12 parameters that further complicated the design process to achieve the best performance. However, the conventional optimization techniques utilized only one or a few factors for simple systems. Therefore, a multi-objective optimization method is proposed in this study by introducing the hybridization of Particle Swarm Optimization and Gravitational Search algorithm (PSOGSA) to optimize the restrainer parameters, as well as to improve the seismic performance of bridges using the optimum design. The optimized MLSR was implemented in the bridge subjected to multi-directional ground motion and its multi-level action to prevent unseating of bridge deck when the applied excitation was evaluated. The optimization process revealed girder displacement in three directions and the number of plastic hinges decreased from 44 to 99% for the optimized design. The time history analysis disclosed that the use of optimized MLSR device decreased the structural seismic response, such as the 3D deck movements, from 79 to 90%. Next, the base shear and drift ratio of bridge bent reduced to 75 and 85% in longitudinal direction and to 72 and 90% in transverse direction, correspondingly. The outcomes signify that the proposed MLSR device and the optimization algorithm have successfully improved the bridge structure resistance against severe ground motions.

Keywords Multi-level spring restrainer (MLSR) · Experimental testing · PSOGSA · Multi-objective optimization · Ground motion · Bridge unseating

1 Introduction

The importance of assessing the structural performance for different types of structures against ground motion is widely acknowledged (Srinivasan Chandrasekaran & Srivastava, 2018; Srinivasan, 2017). Many structural control algorithms for structures equipped with earthquake protection systems have been proposed (Srinivasan Chandrasekaran et al., 2011, 2016; S Chandrasekaran & Roy, 2006). These algorithms can minimize the severe impact of ground motion on the structure by improving the structural performance of the supplementary devices (Adeli & Kim, 2004). Hejazi et al. (2013) developed a structural control algorithm for a structure equipped with viscous damper using the GA technique. The results revealed that the algorithm was effective in mitigating the severe effect of ground motion by reducing the number of plastic hinges occurrence, overall displacement, and rotation of the structure. Shi et al. (2018) introduced an optimization method for TMD considering primary structural damping using artificial fish swarm algorithm (AFSA) technique to minimize the dynamic amplification factor of the structure subjected to harmonic excitation. The optimization method was assessed in pedestrian bridge equipped with optimum TMD. The results showed that the method was more effective in reducing the max dynamic amplification factor than the other tested methods.

✉ Farzad Hejazi
farzad.hejazi@uwe.ac.uk

1   Department of Civil Engineering, University Putra Malaysia, 43400 Serdang, Malaysia

2   Department of Civil Engineering, University of Warith Al-Anbiyaa, Karbala 56001, Iraq

3   Faculty of Environment and Technology, The University of The West England, Bristol, UK

Keykhosro Kiani et al. (2020) presented a combined finite element method (FEM) with multi-objective optimization algorithm using MATLAB-based Tabu search algorithm combined with ABAQUS software to enhance the energy dissipation capacity of a slit type damper. As a result, the developed algorithm was efficient in enhancing the slit damper cyclic performance and the energy dissipation capacity. Bian and Jing (2021) designed a TMD (X-absorber) that demonstrated tunable stiffness and nonlinear damping. The authors achieved the desired behavior by performing a multi-variable optimization technique. It was concluded that the developed absorber was flexible, reliable, and displayed high nonlinear behavior unseen in past studies. (Manuscript length: 8,895 words).

Xian and Su (2022) developed a new hybrid optimization framework for viscous dampers. The researchers considered uncertain device properties and random ground motions. The restrainers are devices used to control structural safety of bridges during seismic events. These devices have different techniques in mitigating the severe impact of earthquake. Some of them could dissipate the earthquake energy, while others limit the girder displacement (Hamzah & Hejazi, 2020, 2022; Shrestha et al., 2016; Xiang et al., 2019). However, the optimization techniques were required to maximize the function of the restrainers and to diminish the severe ground motion effect on bridges.

Prior studies confirmed no algorithm could solve all optimization problems, as some have exploration issue and others have exploitation problem (Lai & Zhang, 2009). Therefore, combining the current optimization techniques is a comprehensive method to stabilize the exploration and exploitation capabilities. Particle Swarm Optimization (PSO) is one of the main evolutionary algorithms in combination methods due to its simplicity, convergence speed, and the ability to search global optimum (Poli et al., 2007). In the last few years, a novel heuristic optimization technique called Gravitational Search Algorithm (GSA) was proposed (Rashedi et al., 2009). This method has the ability of exploitation. However, these algorithms have single capability, either exploration or exploitation. Thus, Mirjalili and Hashim (2010) presented a new hybrid algorithm by combining PSO and GSA algorithms called PSOGSA. This algorithm has both exploration and exploitation capabilities; making it suitable for complex optimization problems. The PSOGSA has been applied in several engineering applications. The PSOGSA was utilized to optimize the design of Reinforced Concrete (RC) frames (Chutani & Singh, 2017). The cost of the beams and columns was considered while optimizing the four-story frame. The results showed that the PSOGSA algorithm addressed the limitations of the PSOGSA.

Turning to this present study, a multi-level spring restrainer (MLSR) had been developed and optimized by using a combination of multiple mechanical springs. The seismic performance of MLSR depends on several parameters that could complicate the optimization process in order to maximize functionality and to diminish the severe effects of earthquake excitation. The current optimization techniques utilize one or a few parameters in Single Degree of Freedom (SDOF) or Multi Degree of Freedom (MDOF) system. However, the structural safety of bridge relied on several factors, such as the failure of bridge components and displacement of each structural node in any direction especially unseating of bridge deck. In addition, optimization techniques should consider many parameters, such as overall seismic responses (displacement), force, and plastic hinges–signifying the need to use multi-objective optimization process to optimize all parameters simultaneously. Therefore, an effective multi-objective optimization algorithm is proposed in this present study by using hybrid PSOGSA. The optimization procedure was applied in the design of bridges equipped with MLSR by considering the MLSR parameters and seismic response of bridge.
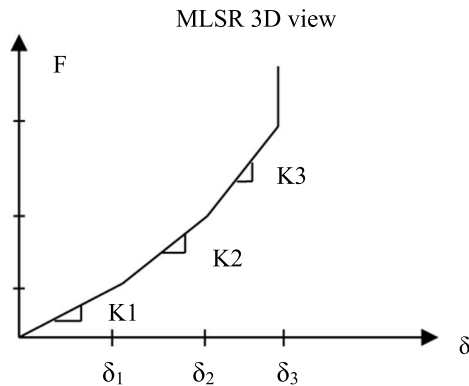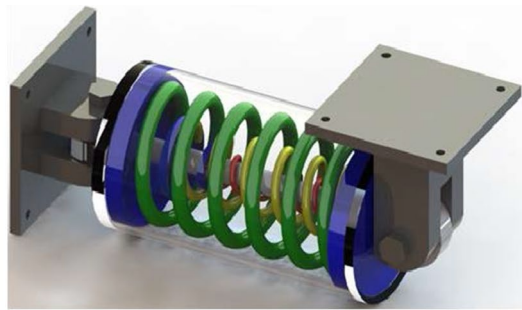
2 The Multi-Level Spring Restrainer (MLSR)

The MLSR mainly consists of multiple mechanical springs with various lengths positioned in parallel to provide multi-level stiffness, as illustrated in Fig. 1. The bridge girder movement is controlled based on its displacement during applied dynamic loads. The restrainer with low stiffness can shift the bridge fundamental period away from the earthquake dominant period. Moreover, the restrainer with high stiffness prevents the bridge failure during severe seismic excitation. The other components of MLSR are the steel covers attached to both ends of each spring to control each spring displacement. In addition, a steel shaft is placed in the middle of the MLSR to provide springs re-centering during ground motion.

The stiffness of the restrainer (K_{out}) is low for the first movement of the restrainer since only the outside spring functions until known displacement (δ_1). Next, the stiffness of the restrainer is increased ($K_{out} + K_{mid}$) by the displacement incremental since the middle spring is involved with the outer spring to display high stiffness of the restrainer until (δ_2). With increased displacement, the stiffness of the restrainer ($K_{out} + K_{mid} + K_{in}$) becomes very high as the inner spring functions with other springs until the third displacement is reached (δ_3). After that, the restrainer is converted to a rigid restrainer and provides ultimate stiffness since all the springs are compressed and reach the solid length to exhibit unseating prevention of bridge girder.

The stiffness equations of the MLSR are:

When $\delta \leq \delta_1, k = k_{out}$

MLSR 3D view

MLSR working mechanism

- If $\delta \leq \delta_1$ $K_d = K_{out}$
- If $\delta_1 < \delta \leq \delta_2$ $K_d = K_{out} + K_{mid}$
- If $\delta_2 < \delta < \delta_3$ $K_d = K_{out} + K_{mid} + K_{in}$
- If $\delta = \delta_3$ $K_d = $ Ultimate

*Note: K_d is the stiffness of MLSR K_{out}, K_{mid}, K_{in} are the stiffness of outer, middle and inner spring respectively

Fig. 1 Multi-level spring restrainer (MLSR)

$$k_d = \frac{Gd_{out}^4}{8D_{out}^3 n_{out}} \tag{1}$$

When $\delta_1 < \delta \leq \delta_2$, $k = k_{out} + k_{mid}$

$$k_d = \frac{D_{mid}^3 n_{mid} Gd_{out}^4 + D_{out}^3 n_{out} Gd_{mid}^4}{8D_{out}^3 D_{mid}^3 n_{mid} n_{out}} \tag{2}$$

When $\delta_2 < \delta \leq \delta_3$, $k = k_{out} + k_{mid} + k_{in}$

$$k_d = \frac{D_{mid}^3 D_{in}^3 n_{mid} n_{in} Gd_{out}^4 + D_{out}^3 D_{in}^3 n_{out} n_{in} Gd_{mid}^4 + D_{out}^3 D_{mid}^3 n_{out} n_{mid} Gd_{in}^4}{8D_{out}^3 D_{mid}^3 D_{in}^3 n_{out} n_{mid} n_{in}} \tag{3}$$

where d = wire diameter, D = mean diameter, n = number of coils, G = Shear modulus.

Equation (3) derived from K_d is considered as a constitutive model for the developed MLSR device and it is applicable to any finite element program.

3 Manufacturing of Prototype and Experimental Testing

The prototype of MLSR was manufactured and tested to assess the restrainer capacity and functionality. The properties of each spring are listed below.

- Inner spring wire diameter (d_{in}): 20 mm, mean diameter (D_{in}): 80 mm, no. of coils (n_{in}): 9, length (L_{in}): 250 mm
- Middle spring wire diameter (d_{mid}): 22 mm, mean diameter (D_{mid}): 150 mm, no. of coils (n_{mid}): 7, length (L_{mid}): 280 mm
- Outer spring wire diameter (d_{out}): 25 mm, mean diameter (D_{out}): 230 mm, no. of coils (n_{out}): 6, length (L_{mid}): 310 mm

The restrainer parts, such as springs, covers, shaft, and outer cover, were provided and assembled to form the prototype. To test the MLSR prototype, a high-capacity actuator was used. Figure 2 illustrates the fabrication, experimental setup for MLSR prototype and the restrainer during the test. The restrainer was installed between the support steel frame and the actuator link. For both connections, welding process was utilized. The restrainer outer cover was welded to the support frame that was attached to the lab strong ground. On other side, the restrainer was linked to the actuator using a steel link element that connected it to the restrainer using a strong steel bar. The designed restrainer maximum displacement was 100 mm and the prototype was tested using the push-and-release method. During the test, the actuator moved first to move the steel link along with the restrainer. At a moment, only the outer spring functioned and provided low stiffness until the movement reached 30 mm. When the displacement increased, the middle spring started to work together with the outer spring until 60 mm displacement and the restrainer stiffness had enhanced. With increased displacement, the inner spring involved the other springs to display the restrainer high stiffness capacity until 100 mm. Next, the loading was released and all the springs returned to their original place.

Figure 3 presents the load displacement curve during loading and unloading of the prototype. As mentioned earlier, the performance of MLSR had been varied. In the initial displacement range, only the first spring was involved. The increment in displacement at the second and third ranges engaged two other springs in sequence for the device function. When the MLSR device began to load, only one spring was included in the functioning of device. A low resistance force at 5 KN
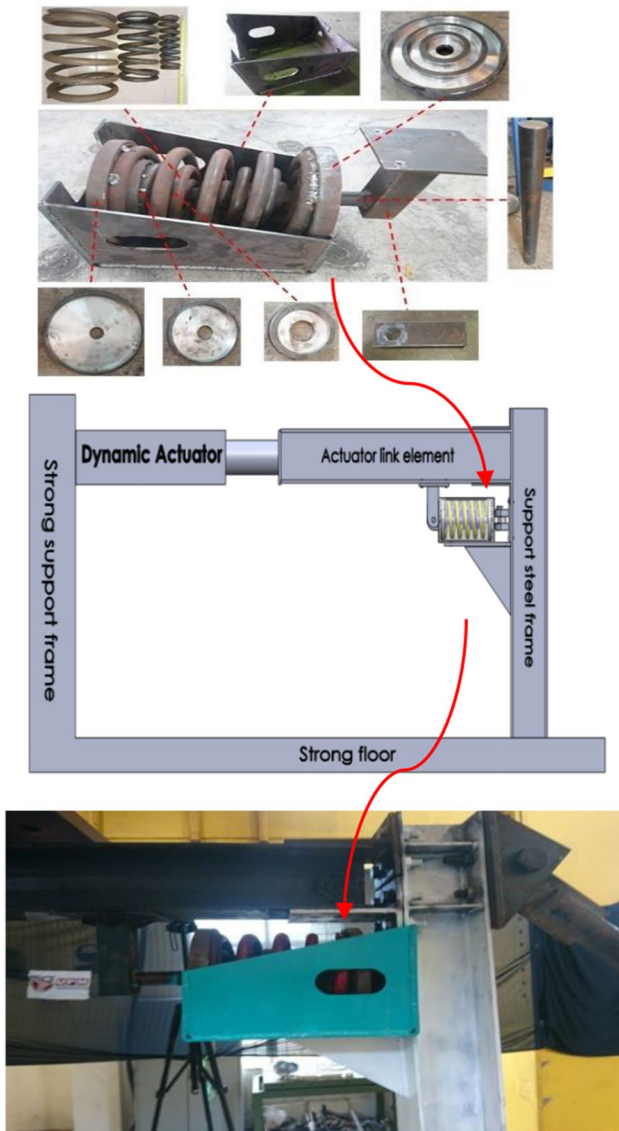
Fig. 2 MLSR fabrication, experimental setup and testing

Fig. 3 Load displacement curve of MLSR prototype

exhibited up to 30 mm displacement. By increasing the load and applying more displacement, the other two springs were involved in the function of device in a sequence depending on the applied displacement ranges. The operation revealed additional resistance force to MLSR device, which resulted in high steep slope curve at higher displacement ranges.

The device resistance improved when the middle spring was included and the capacity reached to almost 10 KN. As a result, the restrainer capacity exceeded 40 KN when the displacement reached 100 mm as all the springs worked together to demonstrate high stiffness. On the other hand, unloading of the prototype reduced the applied displacement. In certain ranges, the engagement of one or two springs was released and this action lowered the force capacity.
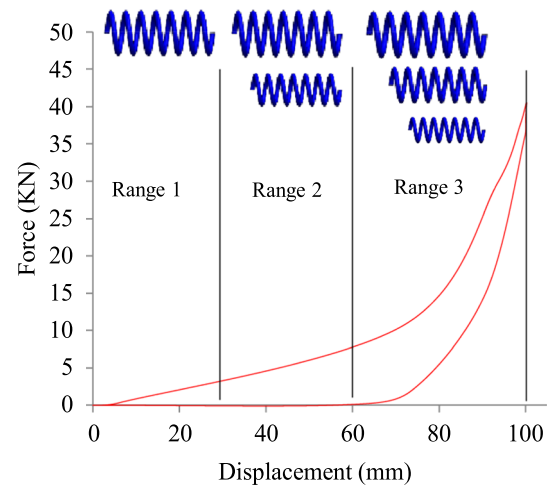
The experimental testing validated the constitutive model of the restrainer. For the first range, the experimental force was 2.8 KN and the force from the constitutive model was 2 KN; showing a slight variance between them. For the second range, the experimental and constitutive model forces were 8.00 KN and 8.59 KN, correspondingly; demonstrating almost similar resistance. As for the third range, the difference between them was 13%, since the maximum experimental force was 41 KN in 100 mm displacement and the maximum force from the constitutive model was 46 KN. Hence, the restrainer constitutive model was selected to develop the optimization procedure, to develop the MLSR finite element model, and to bridge the MLSR algorithm with its application in ARCS3D software (ARCS3D, 2015).

4 Optimization of Bridge Equipped with Multi-Level Spring Restrainer

In this study, a new PSOGSA hybrid algorithm is proposed to enhance the exploration and exploitation capabilities to optimize the performance of MLSR in bridge. The design variables, objective function and design constraint, as well as optimization steps are explained in the following:

4.1 Design Variables and Objective Function

The seismic performance of MLSR is highly affected by design parameters, which may minimize the structural effect of earthquake on bridges. As described above, the developed restrainer relies on stiffness, where K_d is the stiffness of MLSR that depends on 12 parameters. The upper and lower limits of each parameter are described below, except for the mean diameter of middle and outer spring that were determined by the software:

- Inner-spring: wire diameter (d_{in}): 5–50 mm, mean diameter (D_{in}): 10–500 mm, no. of coils (n_{in}): 3–15.
- Middle-spring wire diameter (d_{mid}): 5–50 mm, no. of coils (n_{mid}): 3–15.
- Outer-spring wire diameter (d_{out}): 5–50 mm, no. of coils (n_{out}): 3–15.
- Displacement limits (dis_{in}): 10–150 mm, (dis_{mid}): 20–300 mm, (dis_{out}): 30–450 mm.

In order to optimize a bridge with earthquake protection systems, the hybrid technique was applied to address multi-objective problems due to the high capability of accurate hybrid optimization process.

This study considered the effective parameters on bridge seismic response, such as weight and response of bridge, MLSR parameters, and location. The bridge weight was decreased in terms of column and beam area, diameter, and number of bars. This present study considered the 3D displacement in objective function (f_{obj}), and it is defined as a function of X, Y, and Z displacements of the bridge for optimization process, as well as summation of pier and girder (δx, δy, δz, A_C, & A_B).

The bridge response subjected to earthquake excitation was evaluated by performing inelastic time history analyses. The maximum displacements were utilized to calculate the objective functions. In this study, the 3D bridge model with multi-directional ground motion was considered. The displacements took place in different directions and substantially affected the optimization process. The following equations are expressed after considering the impact of bridge weight and 3D displacements on the optimization process:

$$\Delta x = \max\left(dx_{Max}, |dx_{Min}|\right) \tag{4}$$

$$\Delta Y = \max\left(dY_{Max}, |dy_{Min}|\right) \tag{5}$$

$$\Delta Z = \max\left(dz_{Max}, |dz_{Min}|\right) \tag{6}$$

$$A_b = \sum A_p + \sum A_g \tag{7}$$

where d_{Max} and d_{Min} are peak maximum and minimum displacements in three directions. In addition, ΔX, ΔY, and ΔZ are the amplitude of displacement in X, Y, and Z directions, correspondingly. A_b is the bridge total area, A_p is the piers area, and A_g is the girders area. Therefore, the objective functions are:

$$f_{obj}(1) = \left(\Delta x(n) \times \emptyset_x\right) + \left(\Delta Y(n) \times \emptyset_y\right) + \left(\Delta Z(n) \times \emptyset_z\right) + \left(Ab \times \emptyset_{Ab}\right) \tag{8}$$

$$f_{obj}(2) = \Delta x(n) + \Delta Y(n) + \Delta Z(n) \tag{9}$$

To determine the bridge optimum weight and MLSR optimum parameters, Eq. (8) was applied. The optimum MLSR location can be achieved using Eq. (9). Where, $\emptyset_x$, $\emptyset_y$, and $\emptyset_z$ are coefficients used to scale the 3D displacement, while $\emptyset_{AB}$ is for bridge area scale to ensure that both displacement and area exerted similar impact on the proposed objective function.

4.2 Design Constraints

In order to restrict the bridge girder displacement from over-passing the maximum permissible girder movement, the design constraints were applied since hybrid techniques are founded on unconstrained functions. The optimization constraints for this study included the total number of plastic hinges that occurred when applying load to the bridge members during seismic excitations and unloading. The optimization penalty function is identified as:

$$p = \sum_{i=1}^{nc} CPH_i \times PH_i \tag{10}$$

where P = Penalty function, PH_i = total number of plastic hinges, CPH_i = adjusting coefficient for constraints.

Since the hybrid optimization avoided plastic hinges in bridge components as optimization constraint, the adjusting coefficient was considered as a large value. This reduced the bridge deck movements to three directions. The PSOGSA was restrained by the assigned penalty function by forming plastic hinges and excessive displacement. The competency function (Φ) is the summation of penalty function and objective function.

$$\Phi = f_{obj} + p \tag{11}$$

4.3 Procedure of PSOGSA Optimization Algorithm for Bridge Equipped with MLSR

The developed optimization algorithm in MATLAB Platform was integrated with ARCS3D software. The first step of the computational procedure applied in this study is to generate randomly the initial population within upper and lower limits of the MLSR parameters. The bridge characteristics were considered as a candidate solution. The second step is to apply the variables in time history analysis for the bridge equipped with MLSR using the ARCS3D software. After that, gravitational force and constant were determined:

$$G_{(t)} = G_0 X exp^{\left(-\alpha X iter/iter_{max}\right)} \tag{12}$$

$$Rij = \left|\left|X_i(t), X_j(t)\right|\right|2 \tag{13}$$

where α = descending coefficient, G_0 = initial gravitational constant, Iter = current iteration, $iter_{max}$ = maximum number of iterations.

The following equation was used to determine the total force on agent i in problem with dimension d:

$$F_d^i(t) = \sum_{j=1, j\neq i}^{N} rand_j F_{ij}^d(t) \tag{14}$$

where F_{ij}^d is the gravitational force and $rand_j$ is a random number in interval [0, 1]. Next, particles accelerations were identified using the equation expressed in the following:

$$a_i^d(t) = F_i^d(t)/M_{ii}(t) \tag{15}$$

where d represents the problem dimension, t is the specific time, and M_i denotes the object i mass. Next, the best solution in each iteration is updated. After that, all agent velocity is calculated by:

$$V_i(t + 1) = w X V_i(t) + c_1' X rand X ac_i(t) + c_2' X rand X \left(gbest - X_i(t)\right) \tag{16}$$

where $V_i(t)$ and $ac_i(t)$ are agent i velocity and acceleration at iteration t, respectively, $c_j^{\backslash}$ represents coefficient, w denotes weighting function, rand is a random number [0, 1], and gbest signifies the best solution. In the final step, location of agent is determined by:

$$X_i(t + 1) = X_i(t) + V_i(t + 1) \tag{17}$$

As the end criteria are fulfilled, the optimization process stops updating velocities and locations. Figure 4 illustrates the overall developed procedure.

5 Development of Finite Element Program for Bridge with MLSR

As demonstrated in Fig. 5, the development of finite element model of bridge with MLSR device began by identifying the components of bridge, materials, and sections. Next, the static and dynamic loadings, as well as the boundary condition, were defined. The MLSR geometry specification and material properties were identified in input data. Section and fitting analyses were performed to define the yield surface for all bridge components. In the third step, the static and dynamic loadings were applied and nonlinear time history analysis was conducted. Thereafter, the stiffness was determined based on the present displacement, including the multi-level stiffness of MLSR. Next, the inelastic force was calculated and distributed in the next iteration. The effective stiffness was adjusted and the equation that determines

displacement was run. Finally, the convergence criteria were satisfied and the output data were generated.

As mentioned earlier, the stiffness (Kd) of MLSR refers to the function of displacement. Accordingly, the constitutive model for MLSR was developed as a series of equation of stiffness for each considered displacement range. The MLSR was added to the ARCS3D program (ARCS3d, 2015) as a new displacement dependent element by utilizing the FOR-TRAN language. It was crucial to define the stiffness matrix for the MLSR as a 3D link element in the global coordinate. The action of MLSR was in axial direction only. However, in order to define the compatibility of the MLSR element with beams, columns, and slabs/wall elements, the stiffness of MLSR was added to the axial components of the three dimensions of stiffness matrix $[12 \times 12]$ for two nodes link element (6 DOF for each end node) (see Eq. 19). Since this device did not function in other directions (e.g., shear and moment), other components of stiffness matrix were defined as zero.

$$
\begin{bmatrix}
Kd & 0 & 0 & 0 & 0 & 0 & -Kd & 0 & 0 & 0 & 0 & 0 \\
0 & 0 & 0 & 0 & 0 & 0 & 0 & 0 & 0 & 0 & 0 & 0 \\
0 & 0 & 0 & 0 & 0 & 0 & 0 & 0 & 0 & 0 & 0 & 0 \\
0 & 0 & 0 & 0 & 0 & 0 & 0 & 0 & 0 & 0 & 0 & 0 \\
0 & 0 & 0 & 0 & 0 & 0 & 0 & 0 & 0 & 0 & 0 & 0 \\
0 & 0 & 0 & 0 & 0 & 0 & 0 & 0 & 0 & 0 & 0 & 0 \\
-Kd & 0 & 0 & 0 & 0 & 0 & Kd & 0 & 0 & 0 & 0 & 0 \\
0 & 0 & 0 & 0 & 0 & 0 & 0 & 0 & 0 & 0 & 0 & 0 \\
0 & 0 & 0 & 0 & 0 & 0 & 0 & 0 & 0 & 0 & 0 & 0 \\
0 & 0 & 0 & 0 & 0 & 0 & 0 & 0 & 0 & 0 & 0 & 0 \\
0 & 0 & 0 & 0 & 0 & 0 & 0 & 0 & 0 & 0 & 0 & 0 \\
0 & 0 & 0 & 0 & 0 & 0 & 0 & 0 & 0 & 0 & 0 & 0
\end{bmatrix}
\tag{18}
$$

5.1 Application of Reinforced Concrete Bridge

The considered bridge referred to two spans of reinforced concrete simply supported bridge as illustrated in Fig. 6. The span length was 20 m with 8 m width and the bridge bent consisted of 8 m bent cap and three columns with 6 m height. Modeling of bridge members depends on the behavior of each member during ground motion. Since the girder exhibits elastic behavior during earthquake, the required properties to model this component are the Young's modulus for material, cross-sectional area, and moment of inertia. The column bent displayed plastic behavior. Each column was modeled as beam column element with 1.5*1.5 m concrete cross section and reinforced with eight layers of 25 mm diameter steel bars. The bent cap was modeled as a rectangular concrete beam column element (1.5 m width and 0.8 m height) and reinforced with four layers of 25 mm diameter steel bars. The bridge foundation was assumed to have fixed boundary condition
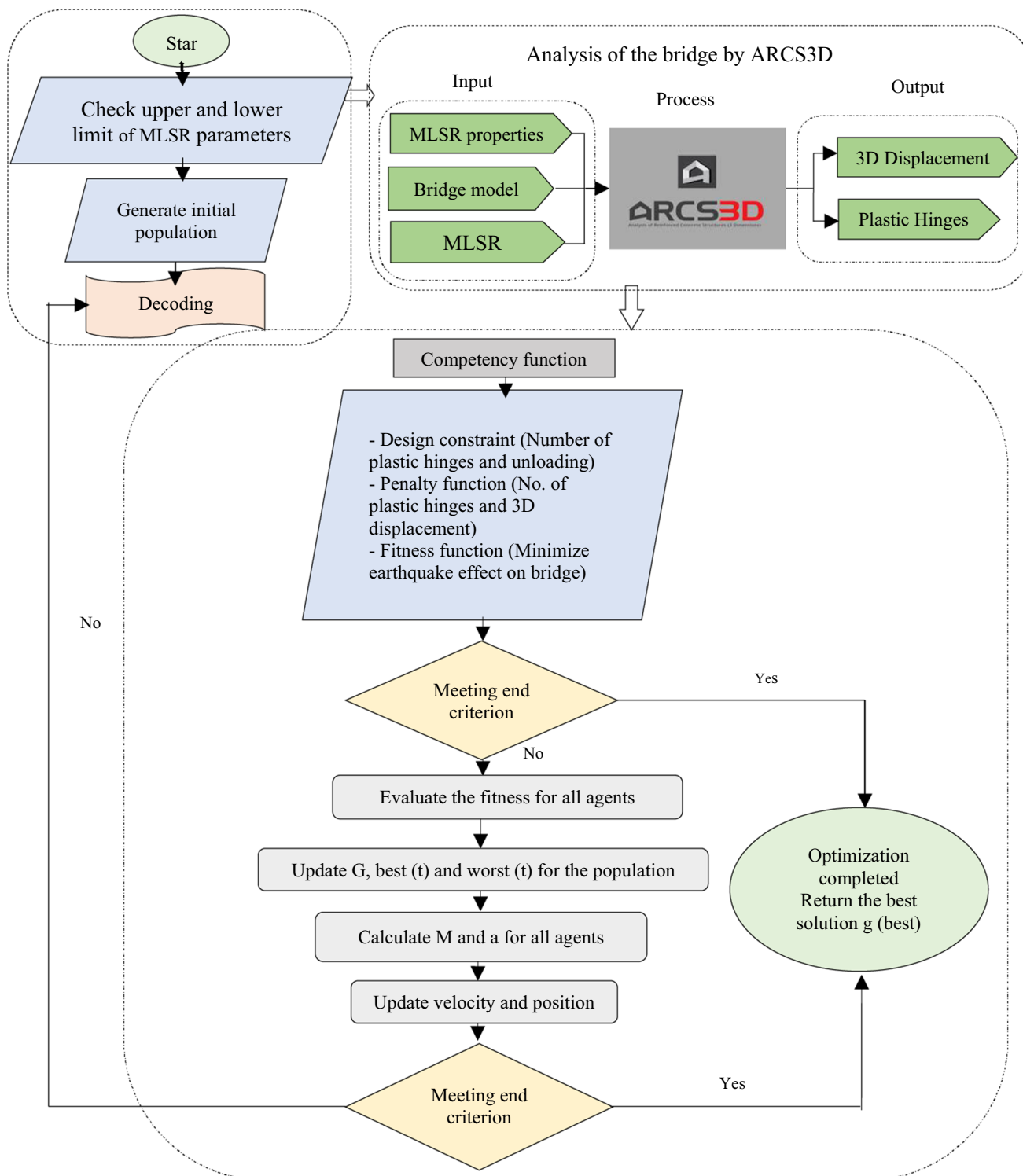
Fig. 4 Procedure of PSOGSA optimization algorithm for bridge equipped with MLSR

and the soil structure interaction was neglected. The FEM time history analysis was performed to evaluate the 3D impact of seismic excitation. Moreover, 3D El-Centro ground motion (1940) that was applied to the bridge.

The 3D bridge numerical model was assessed in terms deck movement and base shear resistance. Next, MLSR was attached to the bridge to improve the bridge seismic performance.
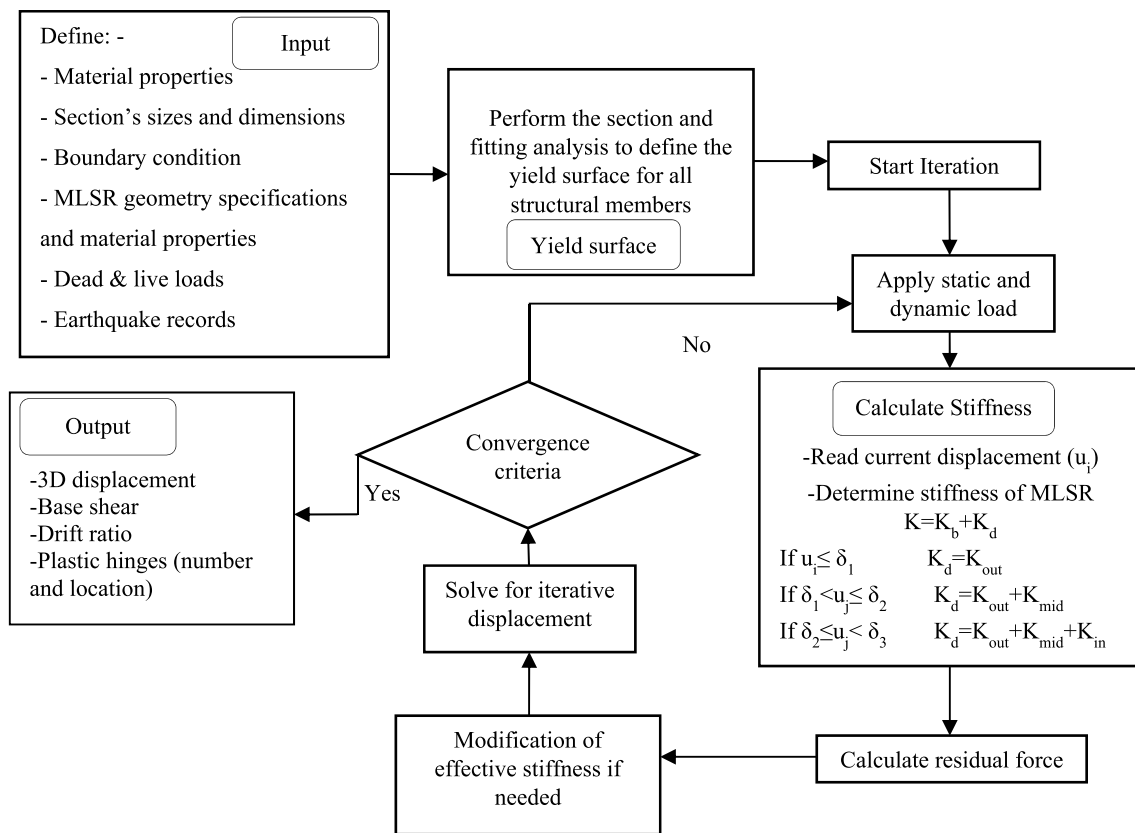
Fig. 5 Computational procedure for bridge equipped with MLSR

The bridge bearing that was considered in the joints reflected partially fixed (elastomeric) bearing. The two methods to model the bearing are micro and macro modeling. In micro modeling, the characteristics of a typical elastomeric bearing (dimensions, elastomer thickness, layers, steel reinforcement, and moment of inertia) are required to display the desired performance. On the other hand, the bearing behavior is needed in macro modeling to describe the bearing performance during applied loading. The bridge in this present study was modeled using macro modeling and the elastomeric bearing nonlinear behavior was achieved by identifying the 3D stiffness (Yura, 2001). The elastomeric bearing in this study was modeled as a stiffener element in the numerical model using the ARCS3D program.

6 Results of Optimization for Bridge with MLSR

The fitness function, the total number of plastic hinge occurrence during the optimization process and the MLSR parameters variation with the number of iteration incremental are illustrated in Fig. 7. During the optimization process, the fitness function was varied and reduced by the number of iteration incremental. At the beginning of the optimization process, the restrainer parameters were selected randomly and the ground motion was applied. Next, the process was repeated until the best bridge response was obtained during applied ground motion. After more than 1000 iterations, the fitness function reduction had stopped and the best solution was attained. Based on the plot, the variation of plastic hinges occurred during loading and unloading of bridge due to vibration stemming from El-Centro ground motion. The plastic hinge reduction was noted from the beginning of the optimization process until around 1000 iterations. The number of plastic hinges reduction was from 400 to less than 50 by the end of the optimization process; signifying 87% declination. This indicates that the PSOGSA algorithm had successfully optimized the restrainer performance to reduce the number of damages in the bridge, while simultaneously providing stability to the bridge. Notably, the most suitable wire diameter for inner spring (d_{in}) is 35 mm to resist El-Centro earthquake excitation for the considered bridge. The mean diameter (D) should be more than or double the wire diameter. Therefore, the mean diameter (D_{in}) for the inner spring was varied based on the wire diameter during the optimization process. Hence, the optimum inner
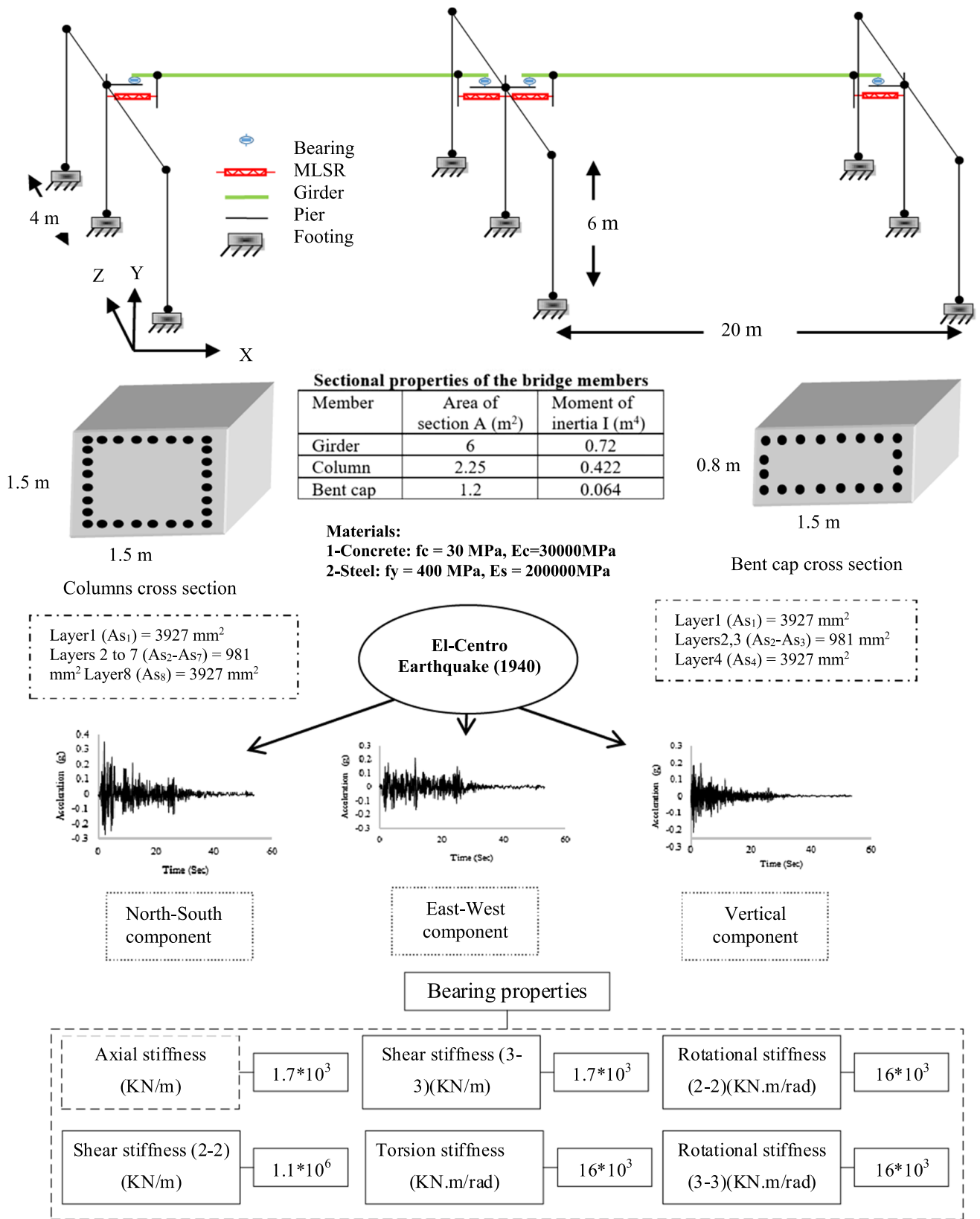
Sectional properties of the bridge members

Member	Area of section A (m²)	Moment of inertia I (m⁴)
Girder	6	0.72
Column	2.25	0.422
Bent cap	1.2	0.064

Materials:
1-Concrete: fc = 30 MPa, Ec=30000MPa
2-Steel: fy = 400 MPa, Es = 200000MPa

Columns cross section

Bent cap cross section

Layer1 (As₁) = 3927 mm²
Layers 2 to 7 (As₂-As₇) = 981 mm² Layer8 (As₈) = 3927 mm²

El-Centro Earthquake (1940)

Layer1 (As₁) = 3927 mm²
Layers2,3 (As₂-As₃) = 981 mm²
Layer4 (As₄) = 3927 mm²

North-South component

East-West component

Vertical component

Bearing properties

| Axial stiffness (KN/m) | 1.7*10³ | Shear stiffness (3-3)(KN/m) | 1.7*10³ | Rotational stiffness (2-2)(KN.m/rad) | 16*10³ |

| Shear stiffness (2-2) (KN/m) | 1.1*10⁶ | Torsion stiffness (KN.m/rad) | 16*10³ | Rotational stiffness (3-3)(KN.m/rad) | 16*10³ |

Fig. 6 The considered bridge details for optimization of MLSR
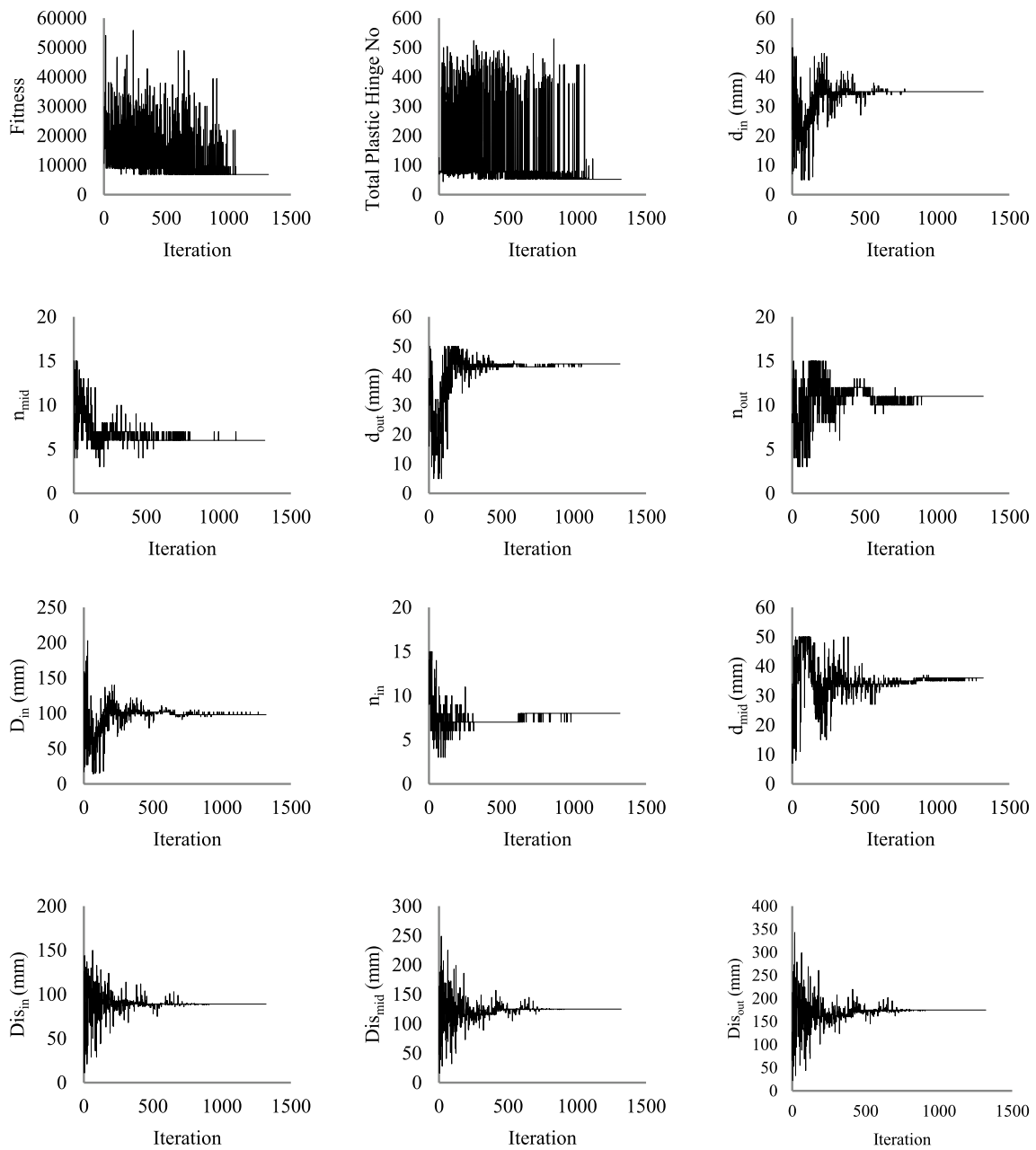
Fig. 7 Fitness function, total number of plastic hinges and MLSR parameters variation during optimization process

spring mean diameter is 98 mm, which is compatible with the best d_{in}.

Similarly, the number of coils of inner spring was varied with the number of iteration incremental until the best solution was attained. The optimum number of coils of the inner spring is 8. For the middle spring, the optimum wire diameter and the number of coils are 36 mm and 6, respectively. The mean diameter of the middle spring was determined during the optimization process based on the inner spring mean diameter and the middle spring wire diameter, whereby the optimum value is 169 mm.

The procedure to reach the optimum parameters of outer spring is similar to that for middle spring. The optimum wire diameter is 44 mm, while the best number of coils for outer spring is 11. The optimum mean diameter for outer spring is 249 mm based on the middle spring mean diameter, as well as the wire diameter of middle and outer springs during optimization. The remaining three parameters are displacement limit for inner, middle, and outer spring. The optimum displacement limit for inner spring is 89 mm, which is the maximum permissible movement for inner spring, for the spring to reach its solid length. The

optimum displacement limit for middle and outer springs are 125 and 175 mm, correspondingly. Hence, the optimum maximum displacement of the restrainer is 175 mm.
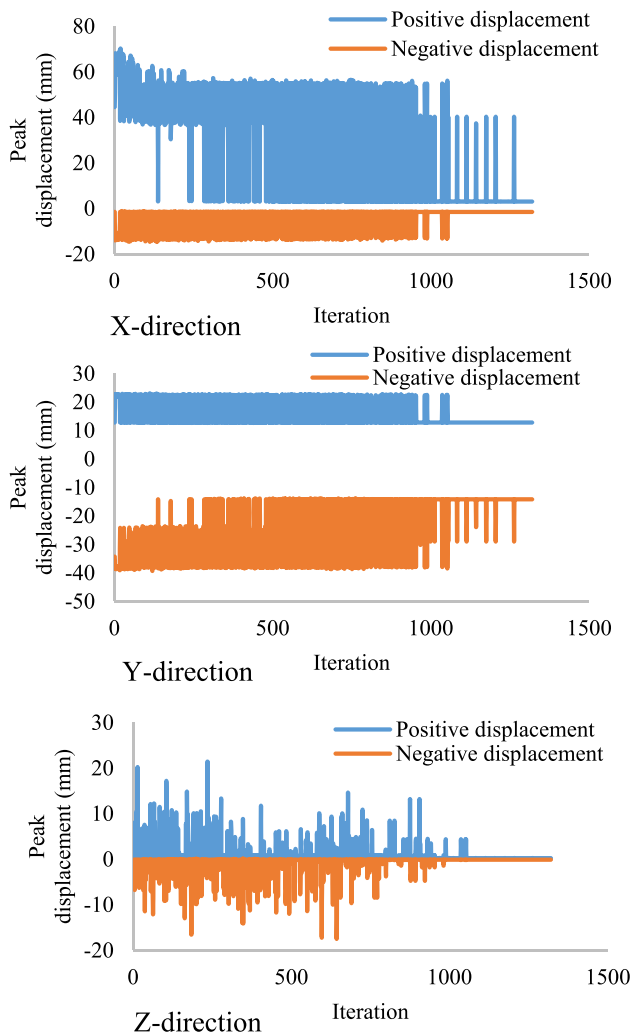

Fig. 8 Peak displacements in X, Y, and Z directions during optimization process

6.1 Bridge Deck Displacement Reduction

The 3D displacement reductions were the optimization objective of this study. Therefore, the 3D displacement results demonstrated variation in optimization of objective function. The maximum and minimum displacements in longitudinal, vertical, and transverse directions during the optimization process are illustrated in Fig. 8. As observed, only the peak positive and negative deck displacements were considered during the seismic excitation. The results revealed that the PSOGSA algorithm had successfully minimized the bridge superstructure movement in all directions. The declination in peak maximum and peak minimum displacements in longitudinal direction were 95 and 92%, correspondingly. The lowered displacements for vertical direction were 44 and 63% for peak maximum and minimum displacements, respectively. Moreover, 98 and 99% were the maximum and minimum peak displacements reduction values, correspondingly.

6.2 Time History Analysis Results for Bridge Without and with the Optimum MLSR

The optimum restrainer was applied in 3D bridge time history analysis in order to assess the efficiency of the restrainer, as well as to evaluate the performance of the bridge components, such as girder displacement, bent base shear, and drift ratio. The displacements of bridge girder in X, Y, and Z directions and the pier base shear responses without and with the optimum MLSR are illustrated in Table 1. The outputs revealed that the bridge response toward El-Centro seismic excitation with the optimum MLSR had improved, while the bridge deck longitudinal displacement reduced by about 85%. In vertical and transverse directions, the superstructure displacements recorded 79 and 90% reduction, respectively. In other words, the unseating of bridge girder was prevented by using the optimum MLSR. The outcomes showed that adding MLSR to the bridge had dramatically reduced the bent shear force. As a result, the bridge with MLSR recorded 75 and 72% reduction in both directions (longitudinal and

Table 1 Maximum girder movement, base shear and drift ratio of bent without/with optimum MLSR

Item	Without optimum MLSR	With optimum MLSR	Reduction	Reduction (%)
Maximum girder displacement (mm) X-direction	71.9	10.9	61.1	0.85
Maximum girder displacement (mm) Y-direction	39	8.3	30.7	0.79
Maximum girder displacement (mm) Z-direction	17.4	1.8	15.6	0.90
Drift ratio in X-direction (%)	1.2	0.18	1.02	0.85
Drift ratio in Z-direction (%)	0.29	0.03	0.26	0.90
Maximum base shear in X-direction (KN)	8415	2102	6313	0.75
Maximum base shear in Z-direction (KN)	3421	957	2464	0.72

transverse). The drift ratio of the pier seemed to improve when the optimum MLSR was applied. Thus, the pier drift ratio reduced from 1.2 to 0.18% in longitudinal direction, while 0.29 to 0.03% reduction in transverse direction.

7 Conclusion

This study proposes the MLSR and an optimization procedure based on Hybrid PSOGSA. An experiment was conducted to validate the numerical model of the proposed restrainer. The 12 characteristics of MLSR were considered as the design parameters, whereas the optimization of objective was identified based on bridge girder 3D displacement. The established optimization procedure denotes a comprehensive computational algorithm, which is applicable to add a new design constraint or objective function. The developed computational procedure was applied to two spans of highway simply supported bridge subjected to 3D ground motion and the optimization outputs were evaluated. The results disclosed that the proposed algorithm had successfully optimized the MLSR and improved the bridge structural resistance against severe ground motions. In other words, the output of the optimization procedure showed substantial reduction in terms of the 3D superstructure movements. In addition, the plastic hinges reduction was 44–99%. The results of nonlinear dynamic finite element analysis revealed that the optimized MLSR reduced the displacement in three directions ranging from 79 to 90%. Next, both base shear and drift ratio of the reinforced concrete columns decreased in longitudinal direction by 75 and 85%, respectively; whereas 72% and 90% in transverse direction for the same, correspondingly. Besides, the optimum MLSR prevented the bridge girder unseating during ground motion event. Future studies may implement another hybrid optimization technique to optimize the seismic performance of MLSR, such as hybrid PSO and GA (HPSOGA) or hybrid ant colony optimization. Moreover, different severe seismic excitation magnitudes can be used to assess the performance of the optimum MLSR in the bridge.

References

Adeli, H., & Kim, H. (2004). Wavelet-hybrid feedback-least mean square algorithm for robust control of structures. *Journal of Structural Engineering, 130*(1), 128–137. https://doi.org/10.1061/(ASCE)0733-9445(2004)130:1(128)

ARCS3D. (2015). Finite element program, analysis of reinforced concrete structures, Copyright by University Putra Malaysia

Bian, J., & Jing, X. (2021). A nonlinear X-shaped structure based tuned mass damper with multi-variable optimization (X-absorber). *Communications in Nonlinear Science and Numerical Simulation, 99*, 105829–106656. https://doi.org/10.1016/j.cnsns.2021.105829

Chandrasekaran, S., & Srivastava, G. (2018). *Design aids of offshore structures under special environmental loads including fire resistance*. Springer Singapore.

Chandrasekaran, S., Nunziante, L., Serino, G., & Carannante, F. (2011). Curvature ductility of RC sections based on Eurocode: Analytical procedure. *KSCE Journal of Civil Engineering, 15*(1), 131–144. https://doi.org/10.1007/s12205-011-0729-4

Chandrasekaran, S., Nunziante, L., Serino, G., & Carannante, F. (2016). *Seismic design aids for nonlinear analysis of reinforced concrete structures*. CRC Press. https://doi.org/10.1201/9781439809150

Chandrasekaran, S., & Roy, A. (2006). Seismic evaluation of multi-storey RC frame using modal pushover analysis. *Nonlinear Dynamics, 43*(4), 329–342. https://doi.org/10.1007/s11071-006-8327-6

Chutani, S., & Singh, J. (2017). Optimal design of RC frames using a modified hybrid PSOGSA. *Algorithm, 63*(4), 123. https://doi.org/10.1515/ace-2017-0044

Hamzah, M. K., & Hejazi, F. (2022). Numerical performance of energy dissipation slotted plate for bridge unseating prevention. *IOP Conference Series: Earth and Environmental Science, 961*(1), 012071. https://doi.org/10.1088/1755-1315/961/1/012071

Hamzah, M. K., & Hejazi, F. (2020). The development of a multi-level unseating prevention device (MLUPD) for bridges. *Structures, 26*, 814–844. https://doi.org/10.1016/j.istruc.2020.05.011

Hejazi, F., Toloue, I., Jaafar, M. S., & Noorzaei, J. (2013). Optimization of earthquake energy dissipation system by genetic algorithm. *Computer-Aided Civil and Infrastructure Engineering, n/a-n/a*. https://doi.org/10.1111/mice.12047

Keykhosro Kiani, B., Hosseini Hashemi, B., & Torabian, S. (2020). Optimization of slit dampers to improve energy dissipation capacity and low-cycle-fatigue performance. *Engineering Structures, 214*, 110609. https://doi.org/10.1016/j.engstruct.2020.110609

Lai, X., & Zhang, M. (2009). *"An efficient ensemble of GA and PSO for real function optimization*. In: Paper presented at the in 2nd IEEE International Conference on Computer Science and Information Technology.

Mirjalili, S., & Hashim, S. Z. M. (2010). *A new hybrid PSOGSA algorithm for function optimization*. In: Paper presented at the 2010 International Conference on Computer and Information Application. https://doi.org/10.1109/ICCIA.2010.6141614

Poli, R., Kennedy, J., & Blackwell, T. (2007). Particle swarm optimization. *Swarm Intelligence, 1*(1), 33–57. https://doi.org/10.1007/s11721-007-0002-0

Rashedi, E., Nezamabadi, S., & Saryazdi, S. (2009). GSA: A Gravitational Search Algorithm. *Information Sciences, 179*, 2232–2248. https://doi.org/10.1016/j.ins.2009.03.004

Shi, W., Wang, L., Lu, Z., & Zhang, Q. (2018). Application of an artificial fish swarm algorithm in an optimum tuned mass damper

design for a pedestrian bridge. *Applied Sciences, 8*(2), 175. https://doi.org/10.3390/app8020175

Shrestha, B., Hao, H., & Bi, K. (2016). Devices for protecting bridge superstructure from pounding and unseating damages: An overview. *Structure and Infrastructure Engineering, 13*(3), 313–330. https://doi.org/10.1080/15732479.2016.1170155

Srinivasan, C. (2017). *Dynamic analysis and design of ocean structures*. Springer.

Xian, J., & Su, C. (2022). Stochastic optimization of uncertain viscous dampers for energy-dissipation structures under random seismic excitations. *Mechanical Systems and Signal Processing, 164*, 108208. https://doi.org/10.1016/j.ymssp.2021.108208

Xiang, N., Goto, Y., Obata, M., & Alam, M. S. (2019). Passive seismic unseating prevention strategies implemented in highway bridges: A state-of-the-art review. *Engineering Structures, 194*, 77–93. https://doi.org/10.1016/j.engstruct.2019.05.051

Yura, J. A. (2001). *Elastomeric Bridge Bearings: Recommended Test Methods*.